



Influence of induced magnetic field and surface roughness of Casson nanofluid flow over an exponentially stretching sheet

Asha S. Kotnurkar^{1,2} · Gayitri Mali^{1,2}

Received: 23 March 2023 / Accepted: 3 July 2023 / Published online: 26 July 2023
© The Author(s) 2023

Abstract

In the present analysis, we have discussed the mixed convective of flow over an exponential sheet in presence of induced magnetic field and surface roughness. The effects of hall current and chemical reaction on flow are also considered. The non-Newtonian model behavior is characterized by Casson nanofluid. The similarity transformations are employed for the transformation of partial differential equations into non-dimensional form and obtained equations are solved by employing the Differential transformation method (DTM). Further, the importance of various parameters on various profiles and gradients are explored graphically with some suitable discussion. At the wall, the small (α) and frequency (n) parameters influence on gradients are illustrated.

Keywords Surface roughness · Exponential stretching sheet · Induced magnetic field · Hall current · Casson nanofluid

Mathematics Subject Classification 35Q35 · 35Q30 · 76-10

List of symbols

x, y	Cartesian coordinates
Re	Local Reynolds number
u, w	Velocity components
$B = B_0 e^{\frac{x}{2L}}$	The magnetic field term
f, g	Dimensionless axial and transvers velocity
C	Nanoparticle volume concentration
T	Temperature of the fluid
C_w	Nanoparticle volume concentration at wall
ρ	Density of the fluid
g^*	Acceleration due to gravity
B_0	The constant magnetic field
Nb	Brownian motion parameter
T_w	Temperature of the fluid at wall
D_B	Brownian diffusion coefficient
Sc	Schmidt number
D_T	Thermophoretic diffusion coefficient
C_∞	Ambient nanoparticle volume fraction
N	Buoyancy ratio

Pr	Prandtl number
U_w	Wall velocity
H_0	Induced magnetic field of strength
μ_e	Magnetic diffusivity
T_∞	Ambient temperature of the fluid
U_0	Reference velocity
H_1, H_2	Components of induced magnetic field
Nt	Thermophoresis parameter

Greek Symbols

α''	Thermal diffusivity
ψ	Stream function
η	Dimensionless similarity variable
θ	Dimensionless temperature
ϕ	Dimensionless nanoparticle volume concentration
β_T	The fluid's volumetric thermal expansion coefficient
β_C	Volumetric solutal expansion coefficient
ν	Kinematic viscosity
ξ	Non-dimensional variable

✉ Asha S. Kotnurkar
ashask@kud.ac.in

¹ Department of Mathematics, Karnatak University, Dharwad, Karnataka 58000, India

² Department of Studies in Mathematics, Karnatak University, Dharwad 580003, India

1 Introduction

A generalized word for the small irregularities in the surface texture of different materials that are frequently created during production is surface roughness. This inquiry is especially important because of how surface roughness affects the rates of heat and mass transfer between both the fluid and the surrounding surface. Several scientific and technological fields use surface roughness, including heat transfer devices, electronic cooling methods, and heat transfer exchangers [1–3]. Numerous researchers have conducted extensive research on the influence of roughness on flows closer to the surface. By examining the changes in heat transfer rates, Smith and Epstein [4] and Kemeny and Cyphers [5] have conducted research on rough surfaces. Surface roughness has been examined by Owen and Thompson [6] using horseshoe-shaped vortices. Furthermore, Dipprey and Sabersky [7] examined how transverse slots affected the flow of fluid. How unnatural roughness influence on heat and motion transfer changes has been studied by Savage and Myers [8]. Townes and Sabersky [9] and Dawson and Trass [10], respectively, explored how surface roughness affected turbulent flow and mass transfer rates. Kandlikar et al. [11] continued the investigation on surface roughness, and their analysis was primarily oriented on fluid flow over small diameter tubes. AbuNada et al. [12] and Sheremet et al. [13] have recently investigated the role of wavy surfaces in improving the efficiency of different transport rates. Additionally, Salimpour et al. [14] focused on the impacts of surface roughness in their study on nanofluid pool boiling.

Keller and Magyari [15] were the first to propose the concept of fluid flow over an exponential sheet. They gave information about the properties of mass and heat transportation as well as numerical solutions over an exponentially sheet. The concept of boundary layer flow caused by exponential sheet is an important consideration in industries and engineering fields such as plastic paper manufacturing, and thinning and annealing of copper wire. The stretched velocity is not always linear, meaning that the stretching fluid's velocity may be nonlinear or exponential. Srinivasacharya and Jagadeeshwar [16] have investigated the flow with hall current effect over an exponentially sheet. The influence of hall currents over an exponential sheet has been studied by Sarojamma et al. [17]. Recently, Asjad et al. [18], Muhammad et al. [19] and Prasannakumara [20] have analyzed the effects of chemical reaction on MHD nanofluid flow due to exponential sheet and the effects of Hall current on nanofluid flow over an exponentially sheet respectively.

When working fluid's magnetic Reynolds number is so small, significance of the induced magnetic field is typically ignored in technical and industrial uses. When the

magnetic Reynolds number ≥ 1 , the impact of the induced magnetic field is actually most noticeable. The investigation of the induced magnetic field becomes important because of its numerous applications in science and the real world, including the production of glass, nuclear reactors, MHD energy generation systems, and so on. The impact of an induced magnetic field on the flow and heat transfer has received very little consideration to date. For instance, Kumari et al. [21] studied the MHD flow and heat transfer under the influence of an induced magnetic field. Recent investigations on induced magnetic field with various geometries are made by Amir Abbas et al. [22], Sahoo and Nandkeolyar [23], and Singh and Vishwanath [24].

The normal conductivity of the magnetic field is deduced to the free spiraling of electrons and ions around the magnetic lines force before colliding when the fluid is an ionised gas and the applied magnetic field is large. At this moment, the magnetic and electric fields both generate a current in a normal path. This process is called Hall effect. In a rarefied medium or a strong magnetic field, the impact of Hall current cannot be disregarded. The analysis of flows involving Hall current has significant industrial uses in a variety of geophysical and astrophysical situations as well as in a number of engineering challenges, including those involving Hall accelerators, Hall effect sensors. It is crucial to examine how Hall current affects fluid flow in the context of these uses. The first person to describe the Hall Effect on two parallel plates in a magnetic field was Sato [25]. Recent studies on Hall Effect are [26–28].

Due to the wide range of applications, the phenomenon of non-Newtonian fluids is receiving a significant amount of attention. One of the most important models that demonstrates the properties of yield stresses among all non-Newtonian liquid models is Casson's fluid flow model, which was first proposed for the flow of non-Newtonian liquids in 1995. The mixing of the solid and liquid phases is the foundation of the Casson liquid model and it behaves like a solid when yield stresses dominate shear stresses. On the other hand, it begins to move when the yield stresses are lower than the shear stresses. Honey, hot sauce, and blood are a few examples of Casson liquids. This flow model finds use in the treatment

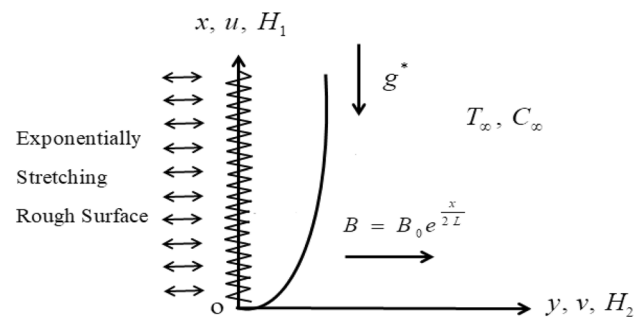


Fig. 1 Schematic diagram of physical problem

of cancer. Nandkeolyar and Prashu [29] have investigated the flow of a Casson fluid. Reddy Konda et al. [30] have studied the mixed convection flow of Casson nanofluid on a nonlinear sheet. Whereas, Prabhakar et al. [31] have discussed the chemical reaction on Casson nanofluid over an exponentially stretching sheet. Numerical solutions of the Casson nanofluid on sheet with porous medium are discussed by Ahmed et al. [32]. Very recently, Suresh Kumar et al. [33] and Sinha et al. [34] investigated the MHD Casson nanofluid flow with various effects.

The net influence of all the previously mentioned factors have not even been tried to be taken into account in any of the above mentioned analyses. The investigation’s main originality and area of interest is how exponential stretching sheets are affected by the Casson nanofluid mixed convective flow under the influence of surface roughness, induced magnetic field, hall current, and chemical reaction. The production of polymer sheets is relevant to the current mathematical modeling. Additionally, these sheets that emerge from the slit during manufacture might not be completely smooth and might have some surface roughness. Such roughness is thought to be modelled by a sine wave form in terms of α and n . Thus, the results of the current analysis are of interest to the design engineers in the polymer industries and assist them by providing the design parameters to control the heat and mass transport rates that decide the ultimate quality of the manufactured product. Here, Differential Transform Method (DTM) is used in the present paper to solve the equations. Without the requirement for an initial guess or discretization, DTM is employed to solve nonlinear ODE problems directly and is undisturbed by discretization defects [35–37]. The influences of relevant parameters on various profiles are provided with appropriate explanation.

2 Mathematical formulation

The surface roughness of Casson nanofluid flow over an exponentially stretching sheet with induced magnetic acting along the vertical channel is shown in Fig. 1.

The governing equations are given below [19, 24, 28, 30]:

The equation for continuity:

$$\frac{\partial u}{\partial x} + \frac{\partial v}{\partial y} = 0, \tag{1}$$

$$\frac{\partial H_1}{\partial x} + \frac{\partial H_2}{\partial y} = 0, \tag{2}$$

$$u \frac{\partial u}{\partial x} + v \frac{\partial u}{\partial y} = v \left(1 + \frac{1}{\beta} \right) \frac{\partial^2 u}{\partial y^2} + g^* \beta_T (T - T_\infty) + g^* \beta_C (C - C_\infty) - \frac{\sigma B^2}{\rho(1+m^2)}(u + mw) + \frac{\mu}{4\pi\rho} \left[H_1 \frac{\partial H_1}{\partial x} + H_2 \frac{\partial H_2}{\partial y} \right], \tag{3}$$

$$u \frac{\partial w}{\partial x} + v \frac{\partial w}{\partial y} = v \left(1 + \frac{1}{\beta} \right) \frac{\partial^2 w}{\partial y^2} + \frac{\sigma B^2}{\rho(1+m^2)}(mu - w) + \frac{\mu}{4\pi\rho} \left[H_1 \frac{\partial H_1}{\partial x} + H_2 \frac{\partial H_2}{\partial y} \right], \tag{4}$$

$$u \frac{\partial T}{\partial x} + v \frac{\partial T}{\partial y} = \alpha'' \frac{\partial^2 T}{\partial y^2} + \tau \left[D_B \frac{\partial C}{\partial y} \frac{\partial T}{\partial y} + \frac{D_T}{T_\infty} \left(\frac{\partial T}{\partial y} \right)^2 \right], \tag{5}$$

$$u \frac{\partial C}{\partial x} + v \frac{\partial C}{\partial y} = D_B \frac{\partial^2 C}{\partial y^2} + \frac{D_T}{T_\infty} \frac{\partial^2 T}{\partial y^2} - (C - C_\infty)K_r, \tag{6}$$

$$u \frac{\partial H_1}{\partial x} + v \frac{\partial H_1}{\partial y} = \mu_e \frac{\partial^2 H_1}{\partial y^2} + H_1 \left(\frac{\partial u}{\partial x} + \frac{\partial w}{\partial x} \right) + H_2 \left(\frac{\partial u}{\partial y} + \frac{\partial w}{\partial y} \right). \tag{7}$$

The boundary conditions are given below [15–17, 19, 24]:

$$u = U_w = U_0 e^{\frac{x}{L}} \left[1 + \alpha \text{Sin} \left(\frac{nx}{L} \right) \right], \quad v = 0, \quad w = 0, \quad H_1 = 0, \quad \frac{\partial H_1}{\partial y} = H_2 = 0, \quad C = C_w, \quad T = T_w \quad \text{at } y = 0, \tag{8}$$

$$u \rightarrow 0, \quad w \rightarrow 0, \quad T \rightarrow T_\infty, \quad C \rightarrow C_\infty, \quad H_1 \rightarrow H_\infty \quad \text{as } y \rightarrow \infty. \tag{9}$$

$$H_\infty = H_0 e^{\frac{x}{L}}$$

Similarity transformations are:

$$\left. \begin{aligned} u &= U_0 \exp \left(\frac{x}{L} \right) f'(\eta), \quad v = -\sqrt{\frac{vU_0}{2L}} e^{\frac{x}{2L}} [f(\eta) + \eta f'(\eta)], \quad T = T_\infty + T_0 e^{\frac{2x}{L}} \theta(\eta), \quad C = C_\infty + C_0 e^{\frac{2x}{L}} \phi(\eta), \\ H_1 &= H_0 e^{\frac{x}{L}} h'(\eta), \quad H_2 = -\sqrt{\frac{v}{2U_0 L}} H_0 e^{\frac{x}{2L}} [h(\eta) + \eta h'(\eta)], \quad \eta = y \sqrt{\frac{U_0}{2vL}} e^{\frac{x}{2L}}, \quad \xi = \frac{x}{L}, \quad \psi = \sqrt{2vU_0 L} e^{\frac{x}{2L}} f(\eta), \\ w &= U_0 e^{\frac{x}{L}} g(\eta), \quad B = B_0 e^{\frac{x}{2L}}. \end{aligned} \right\} \tag{10}$$

where $\psi(x, y)$ is:

$$u = \frac{\partial \psi}{\partial y}, \quad v = -\frac{\partial \psi}{\partial x}$$

$$(1 + \beta)g'' - 2f'g + fg' + \frac{2Ha}{(1 + m^2)}(mf' - g) + 2M\left[(h')^2 - \frac{1}{2}hh'\right] = 0, \tag{11}$$

$$\left(1 + \frac{1}{\beta}\right)f'''' - 2(f')^2 + ff'' + \theta'' + Pr(f\theta' - 4f'\theta + Nb\theta'\phi' + Nt(\theta')^2) = 0, \tag{12}$$

$$-\frac{2Ha}{(1 + m^2)}(f' + mg) + 2\lambda(\theta + N\phi) + \phi'' + Sc(f\phi' - 4f'\phi - 2\phi\chi) + \frac{Nt}{Nb}\theta'' = 0, \tag{13}$$

$$+ 2M\left[(h')^2 - \frac{1}{2}hh'\right] = 0, \tag{14}$$

$$\gamma h''' - hf'' + fh'' - hg' + 2h'g = 0. \tag{15}$$

Simultaneous boundary conditions are

$$\left. \begin{aligned} f(\eta) = 1 + \alpha \sin(n\xi), \quad f = 0, \quad g = 0, \quad h' = 0, \quad h = 0, \quad \theta = 1, \quad \phi = 1 \quad \text{at } \eta = 0, \\ f' \rightarrow 0, \quad g \rightarrow 0, \quad h' \rightarrow 1, \quad \theta \rightarrow 0, \quad \phi \rightarrow 0 \quad \text{as } \eta \rightarrow \infty. \end{aligned} \right\} \tag{16}$$

The parameters are defined as:

$$\left. \begin{aligned} Gr = \frac{g^* \beta_T T_0 L^3}{\nu^2}, \quad N = \frac{\beta_C C_0}{\beta_T T_0}, \quad \lambda = \frac{g^* \beta_T T_0 L}{U_0^2}, \quad Re = \frac{U_0 L}{\nu}, \quad Ha = \frac{\sigma B_0^2 L}{\rho U_0}, \quad M = \frac{\mu H_0^2}{4\pi \rho U_0^2}, \\ Pr = \frac{\nu}{\alpha''}, \quad Nb = \frac{\tau D_B C_0}{\nu} e^{\frac{2x}{L}}, \quad Nt = \frac{\tau D_T T_0}{T_\infty \nu} e^{\frac{2x}{L}}, \quad Sc = \frac{\nu}{D_B}, \quad \gamma = \frac{\mu_e}{\nu}, \quad \chi = \frac{K_0 L}{U_0}. \end{aligned} \right\} \tag{17}$$

3 Method of solution

The reduced governing Eqs. (12)–(16) with (17) are solved by employing DTM method. By employing DTM, we can find the solution of the Eqs. (12)–(16) with (17):

$$\begin{aligned} &(l + 2)\left(1 + \frac{1}{\beta}\right)(l + 1)(l + 3)F(l + 3) - 2 \sum_{q=0}^l (q + 1)(l - q + 1)F(l - q + 1)F(q + 1) \\ &+ \sum_{q=0}^l (l + 1)(l + 2)F(q + 2)F(l - q) - \frac{2Ha}{(m^2 + 1)}((l + 1)F(l + 1) + mG(l)) + 2\lambda(T(l) + NP(l)) \\ &+ 2M\left(\sum_{q=0}^l (q + 1)(l - q + 1)H(l - q + 1)H(q + 1) - \frac{1}{2} \sum_{q=0}^l (l + 1)H(q + 1)H(l - q)\right) = 0, \end{aligned} \tag{18}$$

$$\begin{aligned} &(l + 2)\left(1 + \frac{1}{\beta}\right)(l + 1)G(l + 2) - 2 \sum_{q=0}^l (q + 1)G(l - q)F(q + 1) \\ &+ \sum_{q=0}^l (l + 1)G(q + 1)F(l - q) + \frac{2Ha}{(m^2 + 1)}(m(l + 1)F(l + 1) - G(l)) \\ &+ 2M\left(\sum_{q=0}^l (q + 1)(l - q + 1)H(l - q + 1)H(q + 1) - \frac{1}{2} \sum_{q=0}^l (l + 1)H(q + 1)H(l - q)\right) = 0, \end{aligned} \tag{19}$$

$$(l+1)(l+2)T(l+2) + \Pr \left\{ \begin{array}{l} \sum_{q=0}^l (q+1)T(q+1)F(l-q) - 4 \sum_{q=0}^e (q+1)F(q+1)T(l-q) + \\ Nb \sum_{q=0}^e (q+1)(l-q+1)P(q+1)T(l-q+1) + \\ Nt \sum_{q=0}^e (q+1)(l-q+1)T(q+1)T(l-q+1) \end{array} \right\} = 0, \quad (21)$$

$$(l+1)(l+2)P(l+2) + Sc \left\{ \begin{array}{l} \sum_{q=0}^l (q+1)P(q+1)F(l-q) - 2\chi P(l) - \\ 4 \sum_{q=0}^l (q+1)F(q+1)P(l-q) \end{array} \right\} + \frac{Nt}{Nb}(l+1)(l+2)T(l+2) = 0, \quad (22)$$

$$\begin{aligned} & \gamma(l+2)(l+1)(l+3)H(l+3) - \sum_{q=0}^l (q+1)(q+2)H(l-q)F(q+2) + \\ & \sum_{q=0}^l (l+1)(l+2)H(q+2)F(l-q) - \sum_{q=0}^l (q+1)H(l-q)G(q+1) + 2 \left(\sum_{q=0}^l (q+1)G(l-q)H(q+1) \right) = 0. \end{aligned} \quad (23)$$

The transformation of boundary conditions are:

$$\left. \begin{array}{l} F(0) = 0, \quad F(1) = 1 + \alpha \sin(n\xi), \quad F(2) = \frac{a}{2}, \quad G(0) = 0, \quad G(1) = b, \\ H(0) = 0, \quad H(1) = 0, \quad H(2) = \frac{c}{2}, \quad P(0) = 1, \quad P(1) = d, \quad T(0) = 1, \quad T(1) = e. \end{array} \right\} \quad (24)$$

Differential transform of $f(\eta), g(\eta), \theta(\xi), \phi(\eta)$ and $h(\eta)$ are $F(l), G(l), T(l), P(l)$ and $H(l)$, also with the help of (17), we can find constants a, b, c and e . By utilizing (24) and Eqs. (19)–(23), we get the closed form of solution.

4 Result and discussion

The findings are detailed in Figs. 2, 3, 4, 5, 6, 7, 8, 9, 10, and 11 and displayed to show the features of the problem. The impact of the induced magnetic parameter M on the velocities, temperature, concentration, and induced magnetic profiles is shown in Figs. 2a, 3b, 4a, 5a, and 6a, respectively. As the values of M increases the axial velocity ($f'(\eta)$) profile in Fig. 2a increases, but it resists the transverse velocity ($g(\eta)$) in Fig. 3b. Physically, the induced magnetic field under the influence of the external magnetic field increases the body force and acts as a drag force, accelerating the velocity along the x -axis. The applied magnetic field also

generates a resistive force known as the Lorentz force, which prohibits the $g(\eta)$. In general, a greater estimate of the M , Lorentz force results in a decrease in temperature and concentration. The thickness of the thermal and concentration boundary layer decreases as a result. Hence, temperature and concentration profiles reduce as M rises in Figs. 4a and 5a. When the values of M grow, the thickness of the induced magnetic field boundary layer increases in Fig. 6a. This occurs as a result of the applied magnetic field and induced magnetic field being in the same direction. The influence of the Hartman number Ha on velocities, temperature, and concentration profiles is depicted in Figs. 2b, 3c, 4b and 5b, respectively. According to Fig. 2b, $f'(\eta)$ is decreasing as the value Ha of rises. By applying a uniform magnetic field that is perpendicular to the flow direction, the Lorentz force is generated. The fluid will often move more slowly as a result of this force. Consequently, as Ha is increased, $f'(\eta)$ reduces. As the values of Ha rises, $g(\eta)$ rises in Fig. 3c. The $g(\eta)$ values significantly rise as a result of the Lorentz force, which exerts its influence in the direction of increase in Ha

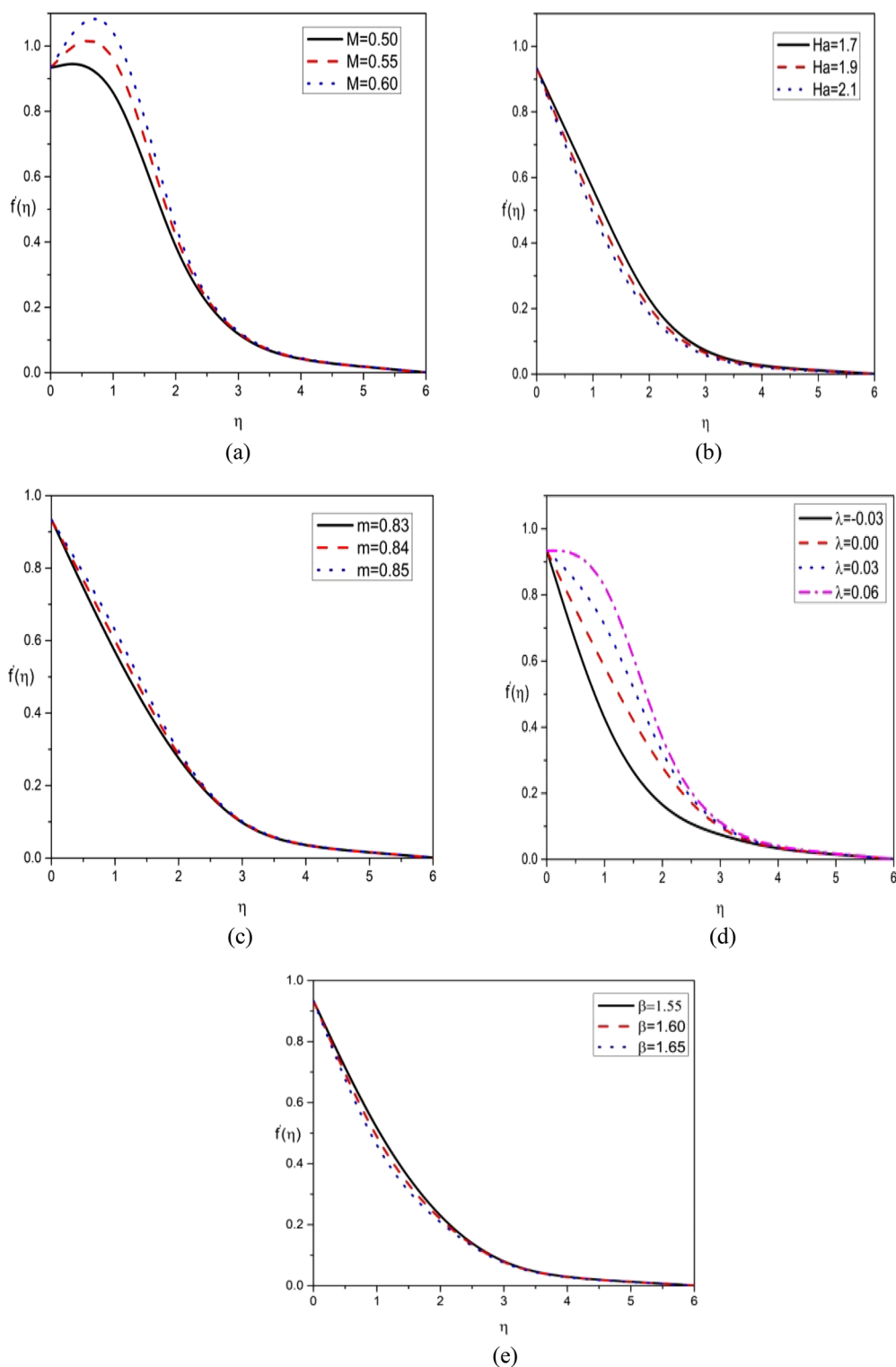


Fig. 2 a–e Variation of $f'(\eta)$. **a** M when $\lambda = 0.1, N = 0.1, m = 0.1, \beta = 0.1, Ha = 0.1, Nb = 0.1, Pr = 2, Sc = 0.5, Nt = 0.1, \alpha = 0.5, n = 50, \xi = 0.5, \gamma = 0.1, \chi = 0.55$. **b** Ha when $\lambda = 0.1, N = 0.1, \beta = 0.1, m = 0.1, M = 0.55, Nb = 0.1, \gamma = 0.1, \alpha = 0.5, n = 50, \xi = 0.5, \chi = 0.55$. **c** m when $\lambda = 0.1, N = 0.1,$

$\beta = 0.1, Ha = 0.1, M = 0.55, Nb = 0.1, Pr = 2, Sc = 0.5, Nt = 0.1, \alpha = 0.5, \xi = 0.5, \gamma = 0.1, \chi = 0.55, n = 50$. **d** λ when $m = 0.1, N = 0.1, \beta = 0.1, Ha = 0.1, M = 0.55, Nb = 0.1, Pr = 2, Nt = 0.1, \alpha = 0.5, \xi = 0.5, n = 50, \gamma = 0.1, \chi = 0.55, Sc = 0.5$. **e** β when $\lambda = 0.1, N = 0.1, m = 0.1, Ha = 0.1, Nb = 0.1, Pr = 2, Sc = 0.5, \alpha = 0.5, n = 50, \xi = 0.5, M = 0.55, \gamma = 0.1, Sc = 0.5, Nt = 0.1$

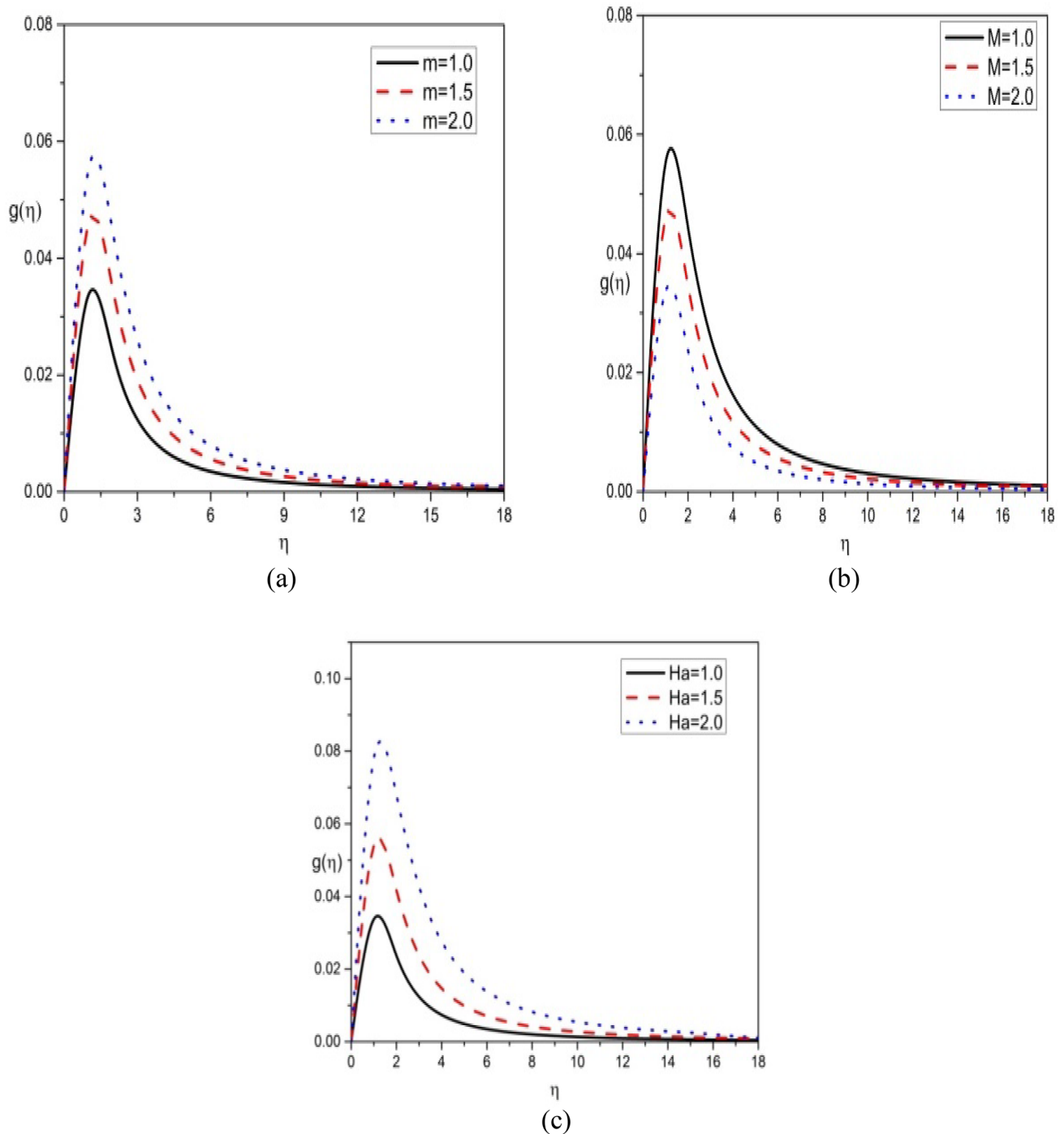


Fig. 3 a–c Variation of $g(\eta)$ on **a** m when $\alpha = 0.5, n = 50, \xi = 0.5, N = 1, \gamma = 0.1, \chi = 0.5, Nt = 0.1, M = 0.5, \lambda = 0.1, \beta = 1, Ha = 1, Nb = 0.1, Pr = 2, Sc = 10$. **b** M when $Nt = 0.1, \lambda = 0.1, \beta = 1, Ha = 1, Nb = 0.1, Pr = 2, Sc = 10, \gamma = 0.1,$

$\alpha = 0.5, n = 50, \xi = 0.5, \gamma = 0.1, \chi = 0.5$. **c** Ha when $\lambda = 0.1, N = 1, M = 0.5, m = 1, \beta = 1, Nb = 0.1, Pr = 2, Sc = 10, \chi = 0.5, Sc = 10, \alpha = 0.5, n = 50, \xi = 0.5, \gamma = 0.1$

values and tends to speed up fluid flow in that direction. The thermal and concentration boundary layer thickens rises as Ha values rise, as shown in Figs. 4b and 5b. By slowing down the fluid's velocity and thickening the thermal and

concentration boundary layer, the magnetic field's application produces a resistive-type force that raises the fluid's temperature and concentration. The impact of Hall parameter m on the velocities, temperature, and concentration

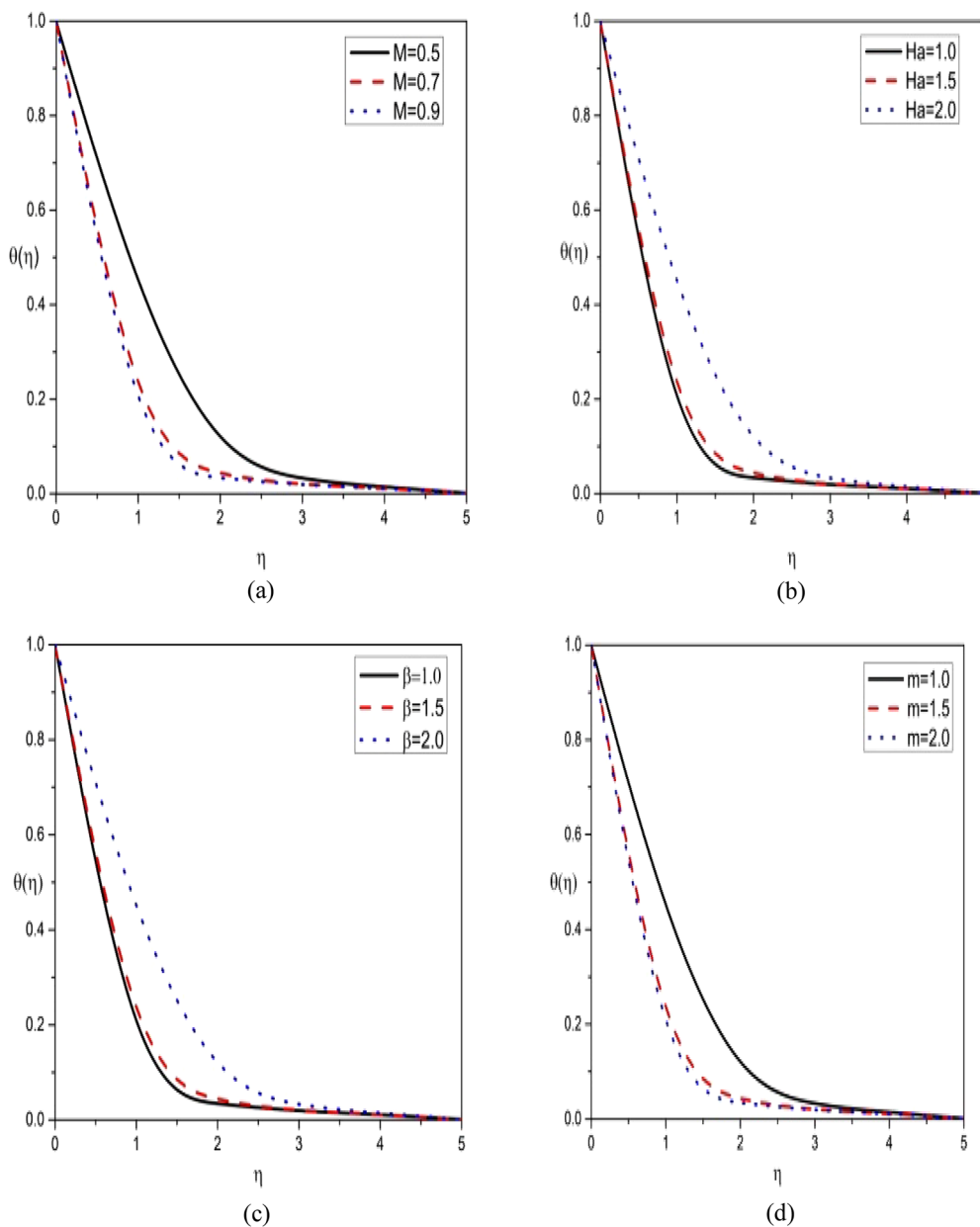


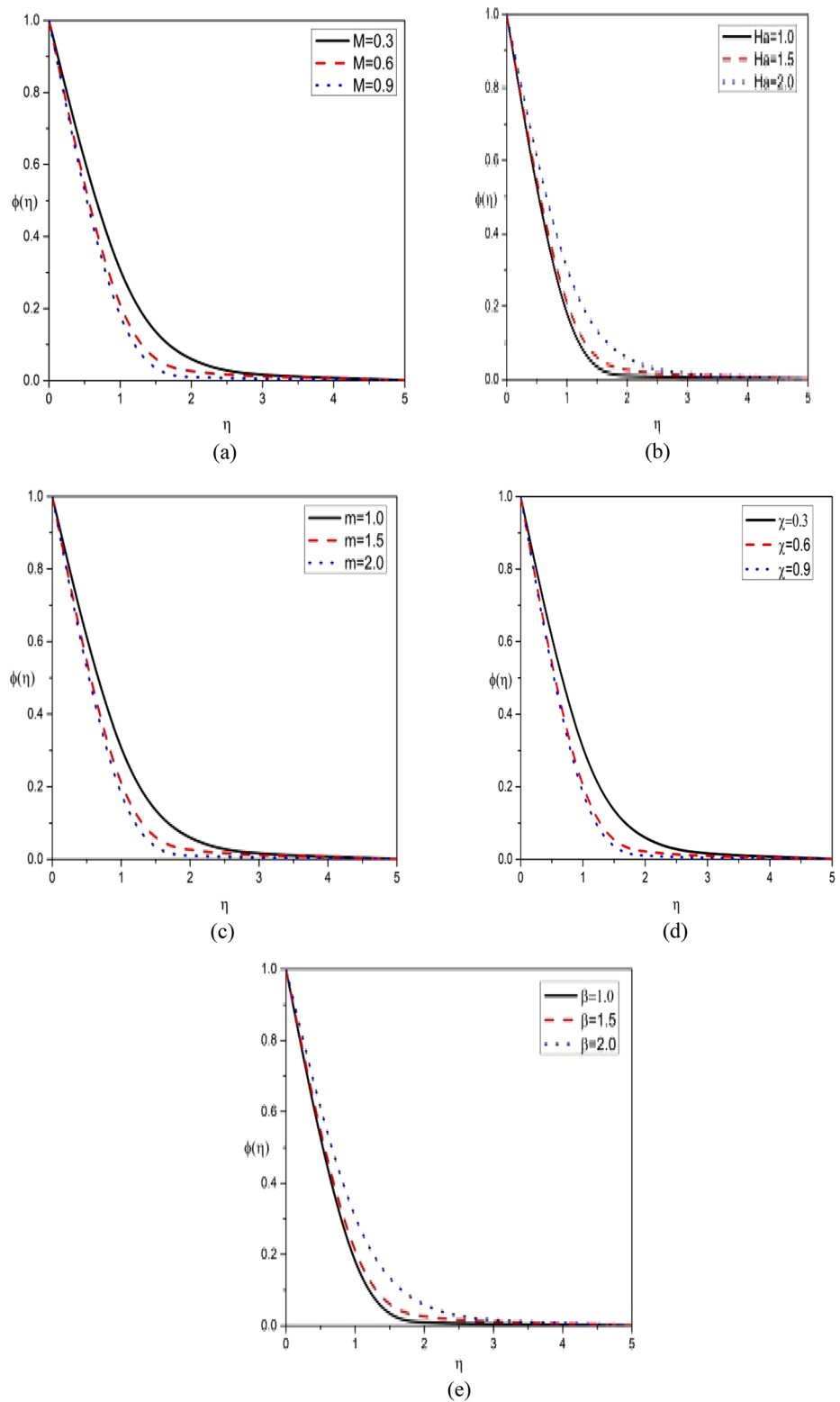
Fig. 4 a–d Variation of $\theta(\eta)$ on **a** M when $\lambda = 0.1, N = 1, m = 1, Ha = 1, Nb = 0.1, Pr = 2, \gamma = 0.1, \beta = 1, Nt = 0.1, Sc = 10, \chi = 0.55$. **b** Ha when $Nt = 0.1, \beta = 1, \lambda = 0.1, N = 1, m = 1, M = 0.55, Nb = 0.1, Pr = 2, Sc = 10, \gamma = 0.1, \chi = 0.55$.

c β when $\lambda = 0.1, N = 1, m = 1, M = 0.55, Nb = 0.1, Pr = 2, Sc = 10, \gamma = 0.1, Ha = 1, \chi = 0.55, Nt = 0.1$. **d** m when $\lambda = 0.1, N = 1, \chi = 0.55, M = 0.55, Nb = 0.1, Pr = 2, Sc = 10, \gamma = 0.1, Ha = 1, Nt = 0.1, \beta = 1$

profiles is shown in Figs. 2c, 3a, 4d, and 5c, respectively. Figure 2c shows that as the values of m enhances, $f'(\eta)$ enhances. Higher values of m decrease the effective conductivity $\frac{\sigma}{1+m^2}$ which, reduces the magnetic damping force on $f'(\eta)$ and this reduction results in an assisting effect on $f'(\eta)$. In Fig. 3a, as the values of m enhances the transverse flow

first enhances gradually with m , reaches a greatest profile and then diminishes. This is due to the fact that for larger values of m , the term $\frac{1}{1+m^2}$ becomes very small and hence resistive effect of the magnetic field is diminished. It is seen from Figs. 4d and 5c that both temperature and nanoparticle volume fraction profiles decrease with increasing m . This is

Fig. 5 a–e Variation of $\phi(\eta)$ on
a M when $Ha = 1$. **b** Ha when
 $\lambda = 0.1, N = 1, \chi = 0.3, Nb = 0.1,$
 $Pr = 2, M = 0.3, Sc = 10, \gamma = 0.1,$
 $\beta = 1, Nt = 0.1$
c β when $\lambda = 0.1,$
 $Nb = 0.1, Pr = 2, Sc = 10,$
 $Nt = 0.1, M = 0.3, Nb = 0.1,$
 $Pr = 2, Sc = 10, Nt = 0.1, Ha = 1,$
 $N = 1, \chi = 0.3, \gamma = 0.1.$
d χ when $Ha = 1,$
 $\lambda = 0.1, N = 1, Nb = 0.1,$
 $Pr = 2, Sc = 10, \gamma = 0.1,$
 $M = 0.3, \beta = 1, Nt = 0.1.$ **e** β when
 $Ha = 1, Nt = 0.1, N = 1, \chi = 0.3, Nb = 0.1,$
 $\lambda = 0.1, M = 0.3, Pr = 2, Sc = 10, \gamma = 0.1$



due to the fact that an increase in m decreases the effective conductivity $\frac{\sigma}{1+m^2}$ and hence the magnetic damping decreases which in turn decreases $\theta(\eta)$, and $\phi(\eta)$. The effect

of Casson fluid parameter β on the axial velocity, temperature, and concentration profiles is shown in Figs. 2e, 4c, and 5e, respectively. In Fig. 2e, it can be seen that by increasing β , axial velocity has decreased. Physically, increase in β causes

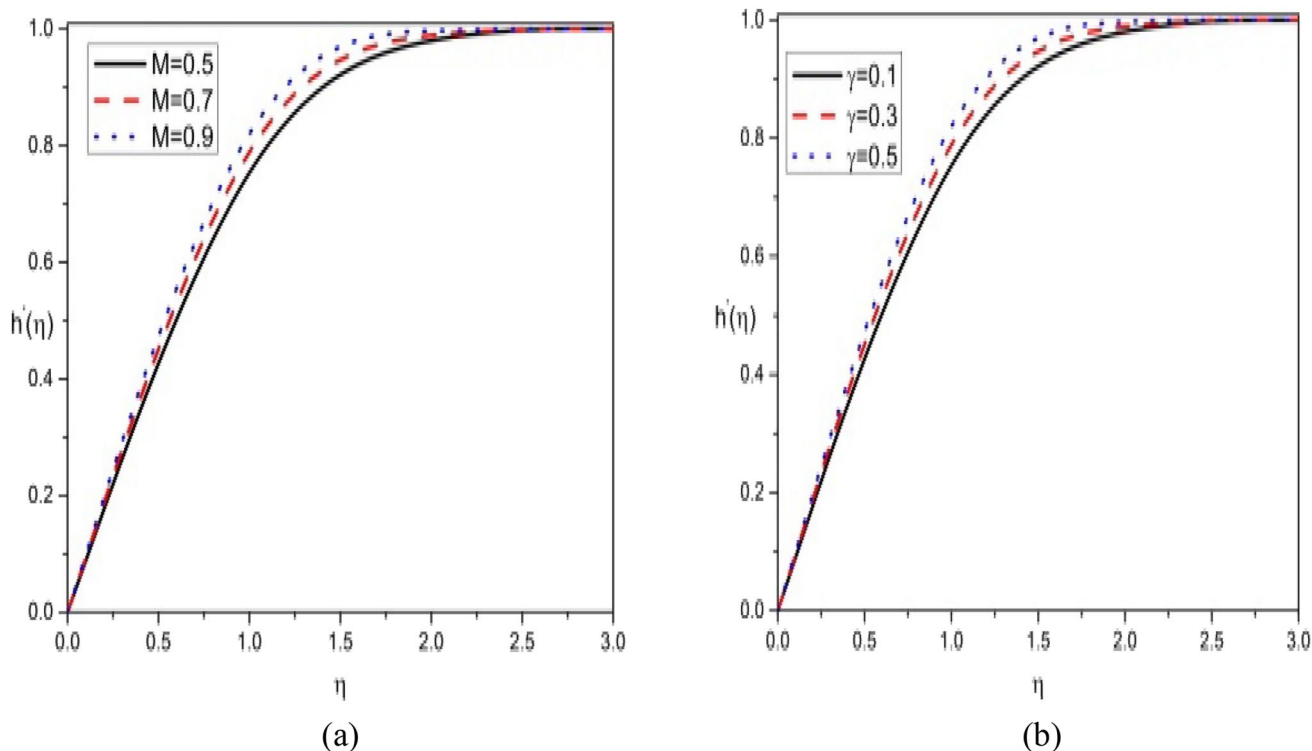


Fig. 6 a, b Variation of $h'(\eta)$ on **a** M when $Nt = 0.1, m = 1.5, \beta = 1, N = 1, \gamma = 0.1, \lambda = 0.1, Ha = 1, Nb = 0.1, Pr = 2, \chi = 0.5, Sc = 10, n = 50, \alpha = 0.5, \xi = 0.5$. **b** γ when

$Nt = 0.1, m = 1.5, \beta = 1, N = 1, M = 0.5, \lambda = 0.1, Ha = 0.1, Pr = 2, \chi = 0.5, Sc = 10, Nb = 0.1, n = 50, \alpha = 0.5, \xi = 0.5, Ha = 0.1$

increase in fluid viscosity, so it is obvious that the higher viscosity results in lower velocity. Also, in Figs. 4c and 5e, it is also observed that the same increase in viscosity has led to an increase in nanofluid temperature and concentrations profiles, respectively. Figure 2d analyses the impact of the mixed convection parameter λ on $f'(\eta)$. It is evident that the dominance of buoyant forces over viscous forces is causing the momentum boundary layer thickness and $f'(\eta)$ to rise. Fig. 5d shows that as the values of chemical reaction parameter χ rises, $\phi(\eta)$ diminishes. It is true because the higher values of chemical reaction make fall in the chemical molecular diffusivity. Fig. 6b shows that as magnetic Prandtl number γ rises, induced magnetic profile ($h'(\eta)$) rises. As γ grows, the magnetic diffusivity declines, which causes the resistive forces to decrease. As a result, the $h'(\eta)$ increases with higher γ .

The variations of the skin-friction coefficient $Re^{\frac{1}{2}} C_f$ along ξ are shown in Figs. 7a–c and 8a–c for various values of small parameter α ($\alpha = 0, 0.03, 0.05, \text{ and } 0.1$) and frequency parameter n ($n = 10, 15, \text{ and } 20$) respectively, for the non-existence and existence of nanoparticles. In particular, the enhancement in α and n considerably enhances the resistance between the wall and fluid particles in Fig. 7a–c, in the absence of nanoparticles. The stretching wall has a greater number of cavities

that may be seen in greater depth due to rising of α and n values. Hence, skin-friction coefficient enhances with values of α and n . The same influences of α and n on $Re^{\frac{1}{2}} C_f$ can be seen in the Fig. 8a–c, when nanoparticles are present. The effects of n ($n = 50, 75, 100$) and α ($\alpha = 0, 0.01, 0.1, 0.2, 0.3, 0.4, 0.5$) on the wall heat transfer rate ($Re^{-\frac{1}{2}} Nu$) along ξ are shown in Figs. 9a–g and 10a–f, respectively, for the non-existence and existence of nanoparticles. In particular, in Fig. 9a–g, the heat transfer rate shows the sinusoidal changes in the occurrence of surface roughness, which increase with the rise in the values of α and n . Heat is transferred from the heated area to the cold one more easily in cavities with more depth. Figure 10a–f show that the presence of nanoparticles causes the heat transfer rate to rise in the direction of the origin, achieve a maximum value, then drop in the opposite direction for larger values of α and n . When nanoparticles are introduced to a fluid, they first collect on a stretched wall, speeding up the rate of heat transfer. Once they have enough energy, they move away from the heated wall after a particular period of time. The heat transfer rate decreases considerably as a result of this. Further, the surface roughness effects are more prominent for $\alpha \geq 0.5$, which can be seen in the Figs. 9a–g and 10a–f. The effects of n ($n = 50, 75, 100$) and α ($\alpha = 0, 0.01, 0.1, 0.2, 0.3, 0.4, 0.5$) on the nanoparticle mass transfer rate ($Re^{-\frac{1}{2}} NSh$) along ξ are shown in

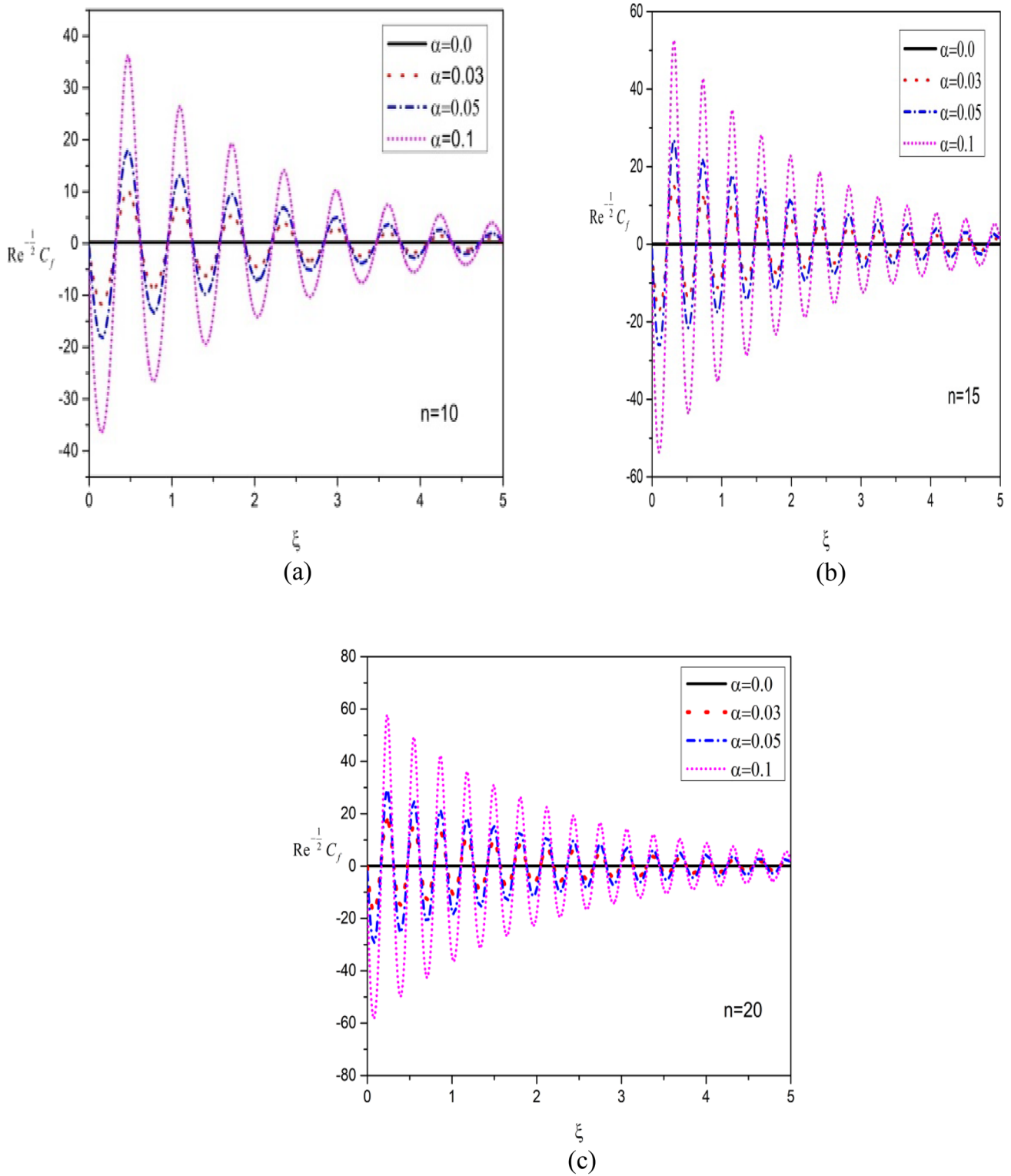


Fig. 7 a–c Effect of α and n on $Re^{\frac{1}{2}} C_f$ for $Nt = 0.0, m = 0.1, \beta = 0.1, \lambda = 10, Ha = 0.1, Nb = 0.0, Sc = 0.0, M = 0.1$

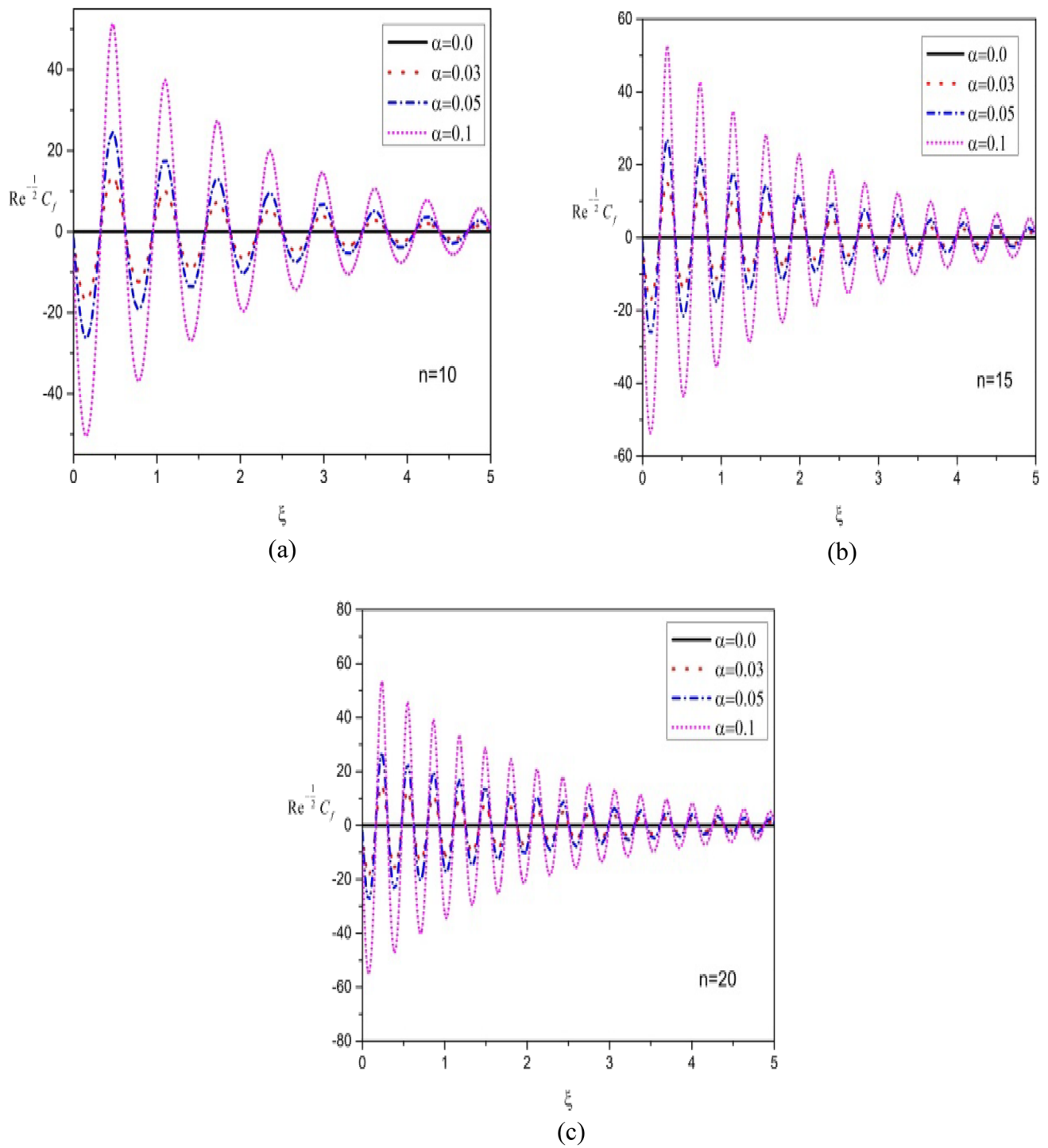


Fig. 8 a–c Effect of α and n on $\text{Re}^{\frac{1}{2}} C_f$ for $Nt = 0.1, m = 0.1, \lambda = 10, \beta = 0.1, Ha = 0.1, Nb = 0.1, Sc = 10, M = 0.1, \chi = 0.1, Pr = 6, N = 0.1$

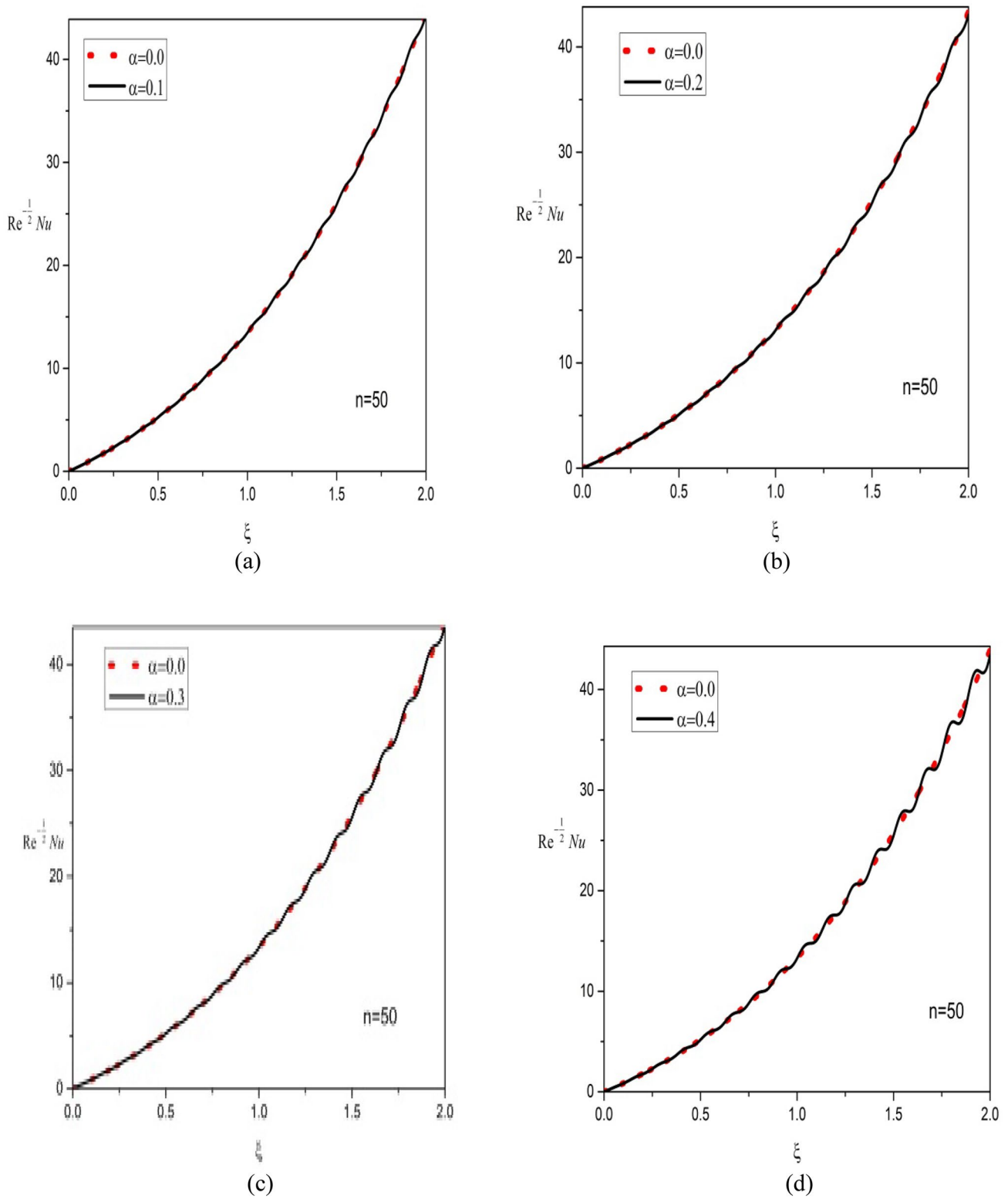


Fig. 9 a–g Effect of α and n on $\text{Re}^{-\frac{1}{2}} Nu$ for $Nt = 0.0$, $\beta = 0.1$, $Ha = 0.1$, $Nb = 0.0$, $Sc = 0.0$, $Pr = 6$, $N = 0.0$

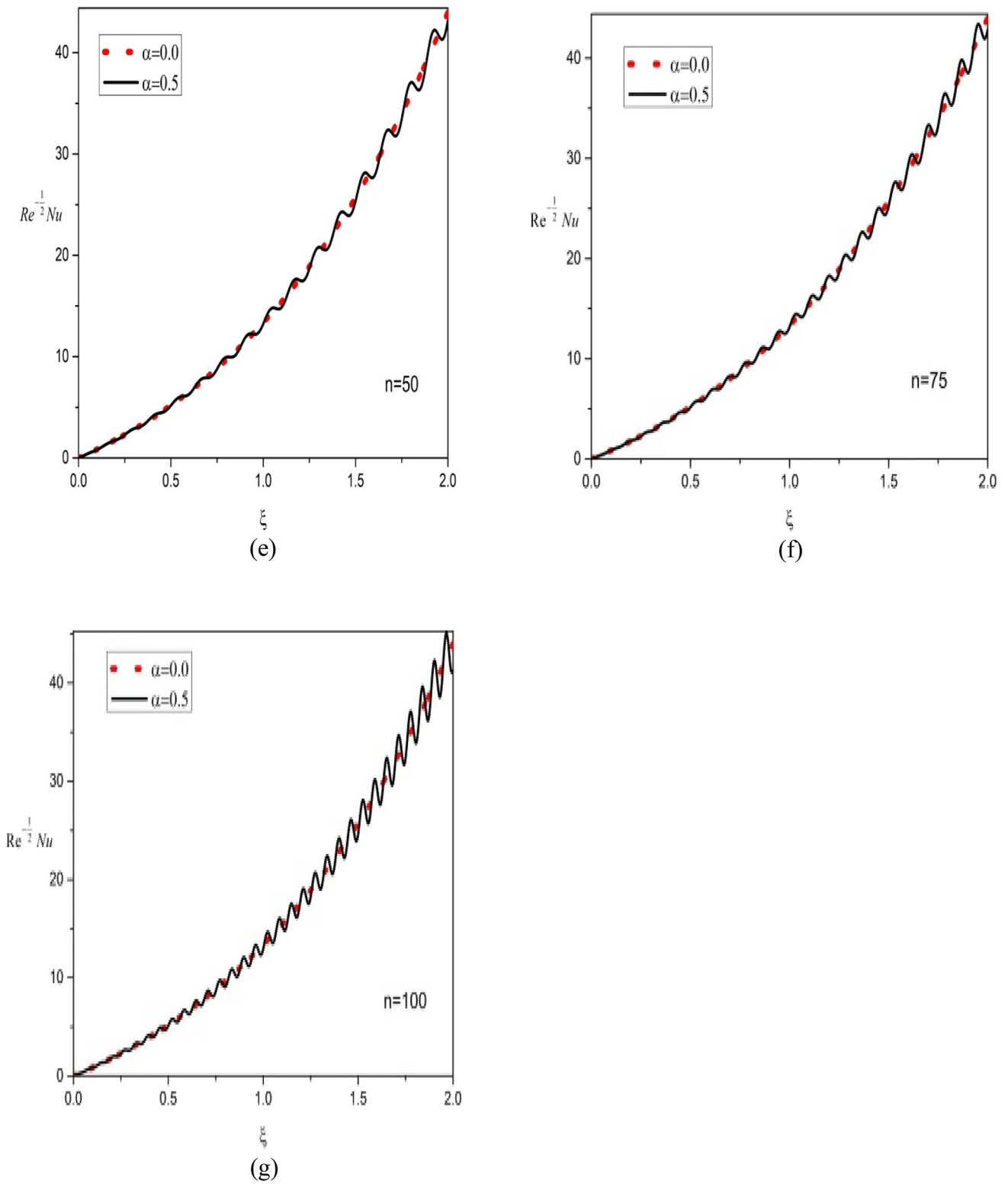
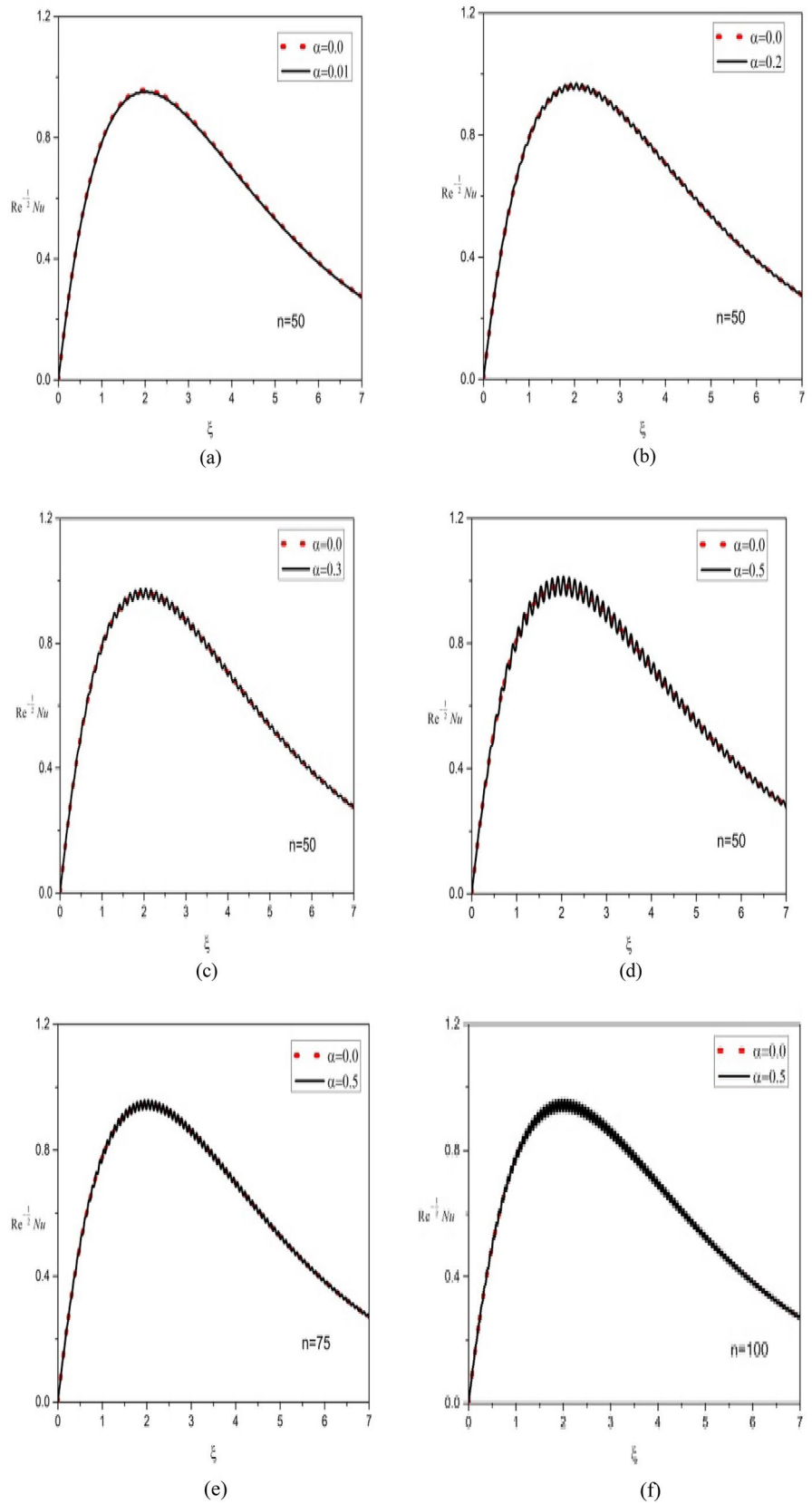


Fig. 9 (continued)

Fig. 10 a–f Effect of α

and n on $Re^{-\frac{1}{2}}Nu$ for

$Nt = 0.1, \chi = 0.1, m = 0.1,$
 $\beta = 0.1, Ha = 0.1, Nb = 0.1, Pr = 6,$
 $Sc = 10,$ and $N = 0.1$



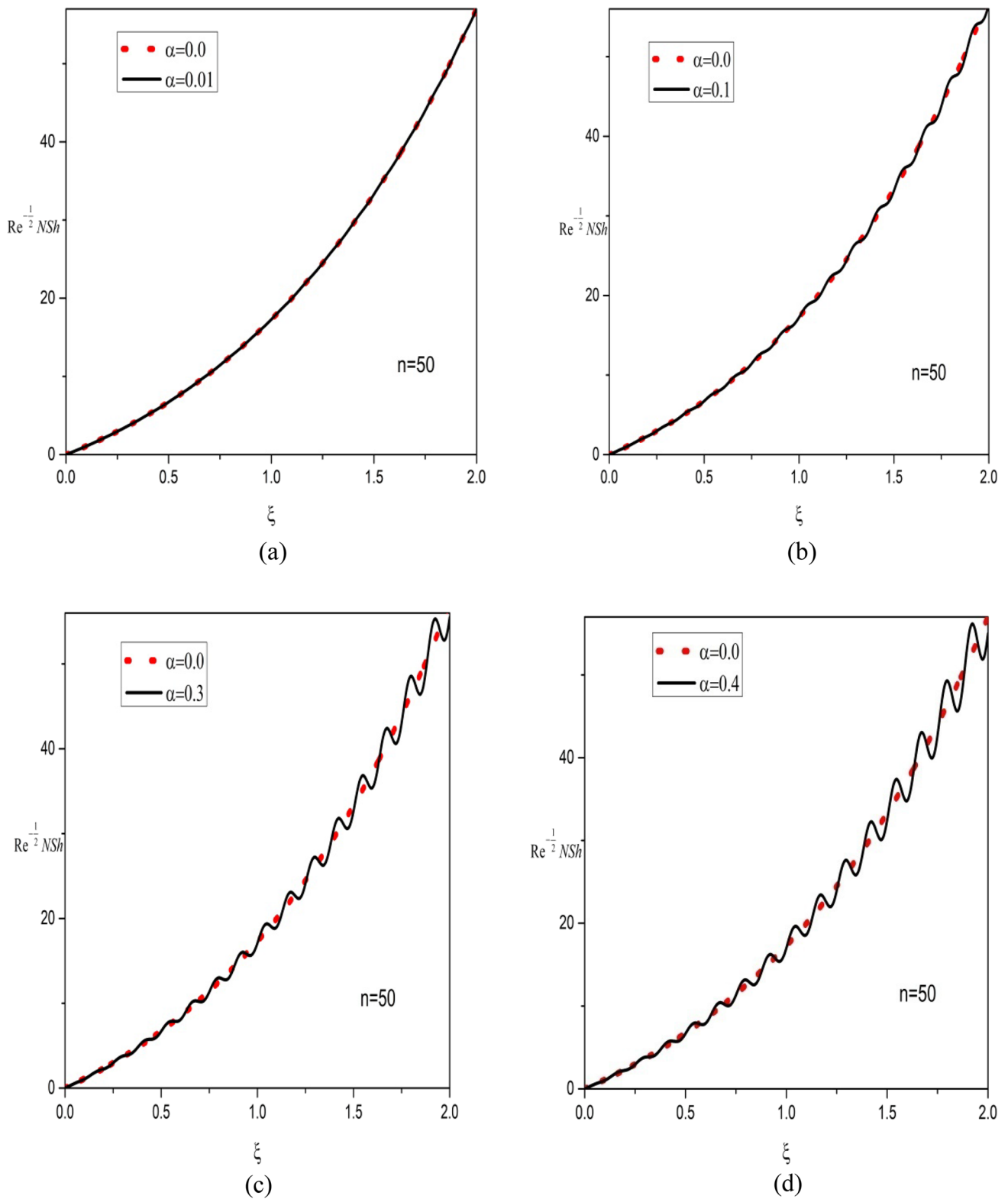


Fig. 11 a–h Effect of α and n on $Re^{-\frac{1}{2}} NSh$ for $Nt = 0.1$, $\chi = 0.1$, $Nb = 0.1$, $Pr = 6$, $Sc = 10$, and $N = 0.1$

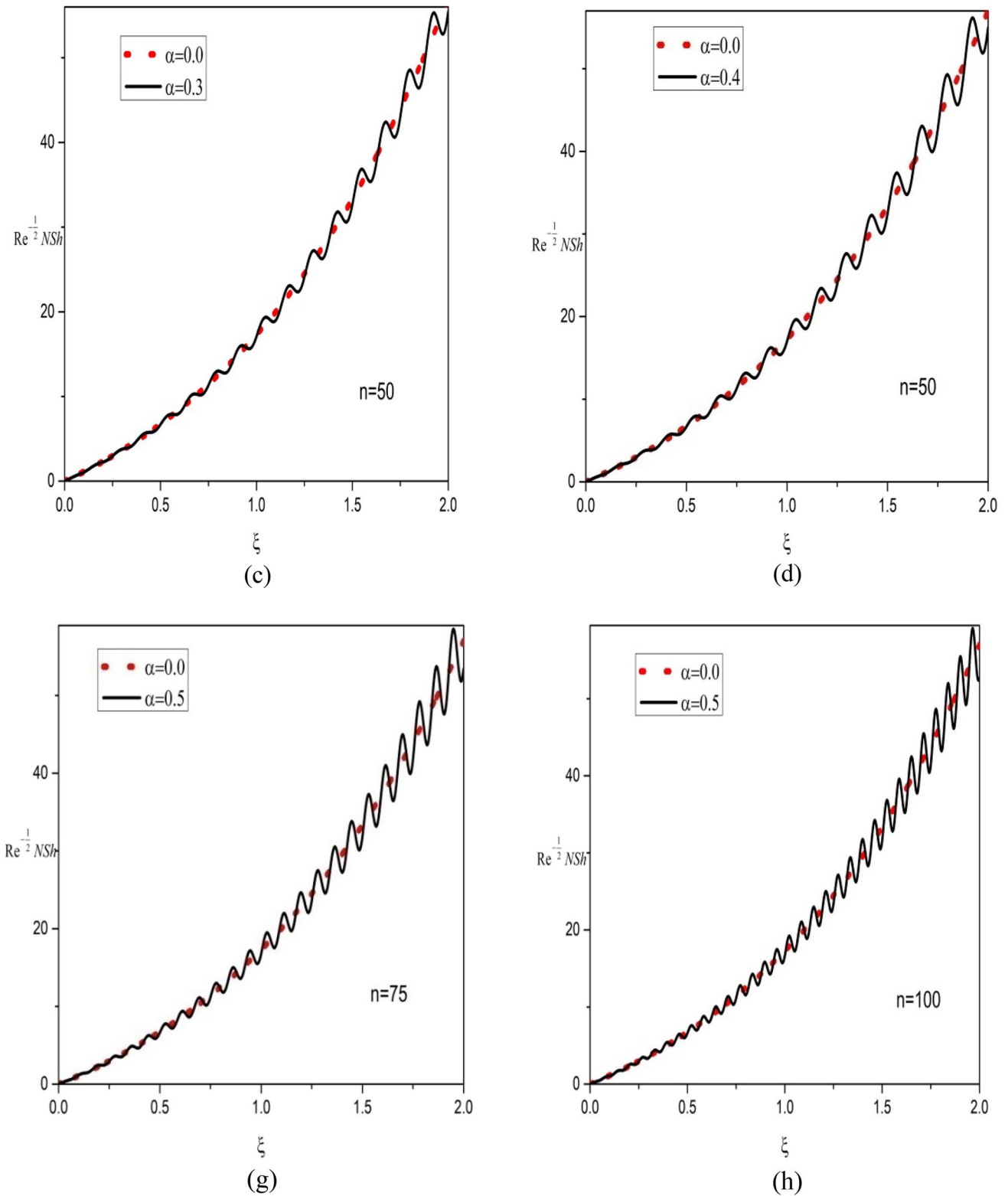


Fig. 11 (continued)

Fig. 11a–h. As values of α and n rise, the magnitude and number of sinusoidal changes in $Re^{-\frac{1}{2}}NSh$ rise, respectively. The wall with a larger surface area and those changes in the mass transfer rate are shown by the greater values of α and n .

5 Conclusions

The current work examines the mixed convective Casson nanofluid flow along an exponential sheet in presence of induced magnetic field, surface roughness, hall current and chemical reaction. The key observations are provided below.

- As values of M enhances, same behavior can be seen in both velocities and induced magnetic profiles but reverse trend can be observed in temperature, volume fraction profiles.
- As values of Ha enhances, same behavior can be seen in the $g(\eta)$, $\theta(\eta)$, and $\phi(\eta)$ profiles, but reverse nature can be seen in $f'(\eta)$ profile.
- As values m enhances, both velocity profiles enhances, but reverse nature can be observed in temperature profile.
- The ambient base fluid's nanoparticles increase friction close to the wall and slow the rate at which heat is transferred from the warm wall to the cool ambient fluid.
- When nanoparticles are introduced to the base fluid, $Re^{-\frac{1}{2}}Nu$ is reduced by around 88% in both smooth ($\alpha = 0$) and rough ($\alpha = 0.5$) surface situations at $\xi = 1$.

Author contributions ASK involved in supervision, writing- reviewing and editing. GM involved in conceptualization, methodology, visualization, investigation, software, data curation.

Funding The authors declare that no funds, grants, or other support were received during the preparation of this manuscript.

Data availability Data sharing not applicable to this manuscript as data sets were not generated or analyzed during the study.

Declarations

Conflict of interest The authors have no relevant financial or non-financial interests to disclose.

Open Access This article is licensed under a Creative Commons Attribution 4.0 International License, which permits use, sharing, adaptation, distribution and reproduction in any medium or format, as long as you give appropriate credit to the original author(s) and the source, provide a link to the Creative Commons licence, and indicate if changes were made. The images or other third party material in this article are included in the article's Creative Commons licence, unless indicated otherwise in a credit line to the material. If material is not included in

the article's Creative Commons licence and your intended use is not permitted by statutory regulation or exceeds the permitted use, you will need to obtain permission directly from the copyright holder. To view a copy of this licence, visit <http://creativecommons.org/licenses/by/4.0/>.

References

1. Gupta D, Solanki SC, Saini JS (1993) Heat and fluid flow in rectangular solar air heater ducts having transverse rib roughness on absorber plates. *Sol Energy* 51:31–37
2. Liu Y, Xu G, Sun J, Li H (2015) Investigation of the roughness effect on flow behavior and heat transfer characteristics in micro channels. *Int J Heat Mass Transf* 83:11–20
3. Zhang Y (2016) Effect of wall surface roughness on mass transfer in a nanochannel. *Int J Heat Mass Transf* 100:295–302
4. Smith JW, Epstein NJ (1957) Effect of wall roughness on convective heat transfer in commercial pipes. *Am Inst Chem Eng J* 3:242
5. Kemeny GA, Cyphers JA (1961) Heat transfer and pressure drop in an annular gap with surface spoilers. *J Heat Transfer* 83:189–197
6. Owenand PR, Thompson WR (1963) Heat transfer across rough surfaces. *J Fluid Mech* 15:321–324
7. Dipprey DF, Sabersky RH (1963) Heat and momentum transfer in smooth and rough tubes at various prandtl numbers. *Int J Heat Mass Transf* 6:329–353
8. Savage DW, Myers JE (1963) The effect artificial surface roughness on heat and momentum transfer. *Am Inst Chem Eng J* 9:694–702
9. Townes HW, Sabersky RH (1966) Experiments on the flow over a rough surface. *Int J Heat Mass Transf* 9:729–738
10. Dawson DA, Trass O (1972) Mass transfer at rough surfaces. *Int J Heat Mass Transf* 15:1317–1336
11. Kandlikar SG, Joshi S, Tian S (2003) Effect of surface roughness on heat transfer and fluid flow characteristics at low reynolds numbers in small diameter tubes. *Heat Transfer Eng* 24:4–16
12. Abu-Nada E, Oztop HF, Pop I (2016) Effects of surface waviness on heat and fluid flow in a nanofluid filled closed space with partial heating. *Heat Mass Transf* 52:1909–1921
13. Sheremet MA, Pop I, Oztop HF, Abu-Hamdeh N (2017) Natural convection of nanofluid inside a wavy cavity with a non-uniform: entropy generation analysis. *Int J Numer Meth Heat Fluid Flow* 27:958–980
14. Salimpour MR, Abdollahi A, Afrand M (2017) An experimental study on deposited surfaces due to nanofluid pool boiling: comparison between rough and smooth surfaces. *Exp Thermal Fluid Sci* 88:288–300
15. Magyariand E, Keller B (1999) Heat and mass transfer in the boundary layers on an exponentially stretching continuous surface. *J Phys D* 32:577–585
16. Srinivasacharya D, Jagadeeshwar P (2017) MHD flow with hall current and joule heating effects over an exponentially stretching sheet. *Nonlinear Eng* 6:101–114
17. Nagalakshmi Ch, Nagendamma V, Shreelakshmi K, Sarojamma G (2015) Effects of hall currents on the boundary layer flow induced by an exponential stretching surface. *Procedia Eng* 127:440–446
18. Asjad MI, Sarwar N, Ali B, Hussain S, Sitthiwirattam T, Reunsumrit J (2021) Impact of bioconvection and chemical reaction on MHD nanofluid flow due to exponential stretching sheet. *Symmetry* 13(12):2334. <https://doi.org/10.3390/sym13122334>
19. Muhammad R, Nazia S, Saleh FA, Hassan Ali SG (2022) Numerical study of nanofluid flow over an exponentially stretching sheet with Hall current considering PEST and PEHF temperatures.

- Waves Random Complex Media. <https://doi.org/10.1080/17455030.2022.2136779>
20. Prasannakumara BC, Shashikumar NS, Venkatesh P (2017) Boundary layer flow and heat transfer of fluid particle suspension with nanoparticles over a nonlinear stretching sheet embedded in a porous medium. *Nonlinear Eng* 6(3):179–190
 21. Kumari M, Takhar HS, Nath G (1990) MHD flow and heat transfer over a stretching surface with prescribed wall temperature or heat flux. *Germany* 25:331–336. <https://doi.org/10.1007/BF01811556>
 22. Aamir Abbas K, Awais A, Sameh A, Ashrafa M, Hijaz A, Muhammad Naveed K (2021) Influence of the induced magnetic field on second-grade nanofluid flow with multiple slip boundary conditions. *Waves Random Complex Media*. <https://doi.org/10.1080/17455030.2021.2011986>
 23. Sahoo A, Nandkeolyar R (2022) Entropy generation analysis on convective radiative stagnation point flow of a Casson nanofluid in a non-Darcy porous medium with induced magnetic field and activation energy: the multiple quadratic regression model. *Waves Random Complex Media*. <https://doi.org/10.1080/17455030.2022.2096270>
 24. Singh JK, Vishwanath S (2021) Hall and induced magnetic field effects on MHD buoyancy-driven flow of Walters' B fluid over a magnetised convectively heated inclined surface. *Int J Ambient Energy*. <https://doi.org/10.1080/01430750.2021.1909652>
 25. Sato H (1961) The hall effect in the viscous flow of ionized gas between two parallel plates under transverse magnetic field. *J Phys Soc Jpn* 16:1427–1433
 26. Trivedi M, Otegbeye O, Ansari MdS, Motsa SS (2019) a paired quasi-linearization on magnetohydrodynamic flow and heat transfer of Casson nanofluid with hall effects. *J Appl Comput Mech* 5:849–860
 27. Deebani W, Tassaddiq A, Shah Z, Dawar A, Ali F (2020) Hall effect on radiative Casson fluid flow with chemical reaction on a rotating cone through entropy optimization. *Entropy* 22:480
 28. Shateyi S, Marewo GT (2014) On a new numerical analysis of the Hall effect on MHD flow and heat transfer over an unsteady stretching permeable surface in the presence of thermal radiation and heat source/sink. *Boundary Value Probl*. <https://doi.org/10.1186/s13661-014-0170-y>
 29. Nandkeolyar R, Prashua (2018) A numerical treatment of unsteady three-dimensional hydromagnetic flow of a Casson fluid with Hall and radiation effects. *Results Phys* 11:966–974
 30. Reddy Konda J, Madhusudhana NP, Konijeti R (2018) MHD mixed convection flow of radiating and chemically reactive Casson nanofluid over a nonlinear permeable stretching sheet with viscous dissipation and heat source. *Multidiscip Model Mater Struct* 14:609–630
 31. Prabhakar B, Bandari S, Kishore Kumar C (2016) Effects of inclined magnetic field and chemical reaction on flow of a Casson nanofluid with second order velocity slip and thermal slip over an exponentially stretching sheet. *Int J Appl Comput Math* 3:2967–2985
 32. Ahmed SE, Mohamed RA, Ali AM, Chamkha AJ, Soliman MS (2021) MHD Casson nanofluid flow over a stretching surface embedded in a porous medium: effects of thermal radiation and slip conditions. *Lat Am Appl Res* 51:229–239
 33. Suresh Kumar Y, Hussain S, Raghunath K, Ali F, Guedri K, Eldin SM, Khan MI (2023) Numerical analysis of magnetohydrodynamics Casson nanofluid flow with activation energy. Hall current and thermal radiation. *Sci Rep* 13:4021. <https://doi.org/10.1038/s41598-023-28379-5>
 34. Sinha VK, Nandkeolyar R, Singh MK (2023) Numerical simulation and regression analysis of MHD dissipative and radiative flow of a Casson nanofluid with Hall effects. *Waves Random Complex Media*. <https://doi.org/10.1080/17455030.2023.2168788>
 35. Asha SK, Mali G (2022) Entropy generation and thermal radiation effects on nanofluid over permeable stretching sheet. *J Math Res Appl* 42:523–538
 36. Asha SK, Mali G (2021) Application of differential transform method to triple diffusion convective boundary layer flow of Casson nanofluid over a horizontal plate. *World Sci News* 162:161–178
 37. Sepasgozar S, Faraji M, Valipour P (2017) Application of differential transformation method for heat and mass transfer in a porous channel. *Propuls Power Res* 6:41–48

Publisher's Note Springer Nature remains neutral with regard to jurisdictional claims in published maps and institutional affiliations.